

**Ultrasound-activated microbubbles as a novel intracellular drug delivery system for urinary tract infection**

Horsley, H<sup>1,5</sup>., Owen, J. <sup>2,5</sup>, Carugo, D.<sup>3,4</sup>, Malone-Lee, J<sup>1</sup>., Stride, E<sup>2,6</sup>., and J. L. Rohn<sup>1,6</sup>

- 1. Department of Renal Medicine, Division of Medicine, University College, London, UK
- 2. Institute of Biomedical Engineering, University of Oxford, UK
- 3. Faculty of Physical Sciences and Engineering, University of Southampton, UK
- 4. Institute for Life Sciences, University of Southampton, UK
- 5. These authors contributed equally to the work
- 6. Senior authors to whom correspondence should be addressed

Running Title: Ultrasound-activated microbubbles for intracellular delivery

Keywords: Drug delivery; intelligent delivery; encapsulation; microbubbles; ultrasound; sonoporation; cavitation; chronic infection; intracellular infection; antimicrobial resistance

**Abstract**

The development of new modalities for high-efficiency intracellular drug delivery is a priority for a number of disease areas. One such area is urinary tract infection (UTI), which is one of the most common infectious diseases globally and which imposes an immense economic and healthcare burden. Common uropathogenic bacteria have been shown to invade the urothelial wall during acute UTI, forming latent intracellular reservoirs that can evade antimicrobials and the immune response. This behaviour likely facilitates the high recurrence rates after oral antibiotic treatments, which are not able to penetrate the bladder wall and accumulate to an effective concentration. Meanwhile, oral antibiotics may also exacerbate antimicrobial resistance and cause systemic side effects. Using a human urothelial organoid model, we tested the ability of novel ultrasound-activated lipid microbubbles to deliver drugs into the cytoplasm of apical cells. The gas-filled lipid microbubbles were decorated with liposomes containing the non-cell-permeant antibiotic gentamicin and a fluorescent marker. The microbubble suspension was added to buffer at the apical surface of the bladder model before being exposed to ultrasound (1.1 MHz, 2.5 Mpa, 5500 cycles at 20 ms pulse duration) for 20 seconds. Our results show that ultrasound-activated intracellular delivery using microbubbles was over 16 times greater than the control group and twice that achieved by liposomes that were not associated with microbubbles. Moreover, no cell damage was detected. Together, our data show that ultrasound-activated microbubbles can safely deliver high concentrations of drugs into urothelial cells, and have the potential to be a more efficacious alternative to traditional oral antibiotic regimes for UTI. This modality of intracellular drug delivery may prove useful in other clinical indications, such as cancer and gene therapy, where such penetration would aid in treatment.

## Introduction

Given the limitations of passive diffusion through the plasma membrane, the ability to deliver therapeutic doses of drugs or other compounds to the interior of cells in the body is an important goal for many treatment strategies, including cancer treatment and gene therapy [1]. Chronic bacterial infection is also a particular problem that would benefit from a penetrative drug delivery system, as it can involve intracellular infection [2], or poorly permeable biofilms that are difficult to treat with traditional antibiotics, especially on indwelling devices such as stents or catheters [3].

Urinary tract infection (UTI) is a good example of a chronic infection in need of improved, penetrative treatment modalities. UTI is one of the most common infectious diseases globally, and is the number one infectious disease in our growing elderly population. UTI's sheer prevalence, added to its frequent treatment failures and propensity to recur [4, 5], makes it an immense economic and healthcare burden [6], and one of the most common reasons that general practitioners prescribe antibiotics [7]; indeed, the World Health Organization has issued warnings about common uropathogens in the worsening antimicrobial resistance crisis [8]. There is also evidence that a chronic form of low-level UTI plagues some patients, particularly the elderly, causing less traditional but equally distressing lower urinary tract symptoms including incontinence [9-11]. Moreover, UTI is one of the most prevalent hospital-acquired infections [12], and can lead to more serious complications including kidney infection and urosepsis [13, 14].

As one possible explanation for treatment failure and recurrence, it has emerged that urinary pathogens can form dormant reservoirs within cells, where they may evade luminal antibiotics and the immune system [15]. The most widely studied bacteria in this regard is *Escherichia coli*, which is also the most common uropathogen, responsible for upwards of 80% of all community acquired infections [6]. In mouse models, *E. coli* has been shown to form sophisticated intracellular bacterial communities (IBC) with biofilm-like characteristics inside the apical umbrella cells of the urothelium [15, 16] and dormant quiescent intracellular reservoirs forming deeper within the bladder wall [17]. Other common uropathogens including *Enterococcus faecalis* [18, 19], *Staphylococcus saprophyticus* [20] and *Klebsiella pneumonia* [21] have also been shown to invade and reside within bladder cells, suggesting strong selection pressure for an intracellular lifestyle in the harsh bladder niche.

Given that some widely used antibiotics do not efficiently penetrate mammalian cells [22], and even permeant drugs are unlikely to achieve a therapeutic intracellular concentration if the treatment relies on free diffusion alone [22, 23], oral antibiotic failure in recurrent UTI may well be linked to intracellular reservoir behaviour. We therefore wanted to develop an alternative treatment that could deliver high levels of drug within urothelial cells where it is needed to eradicate sequestered bacteria. In the case of more entrenched or recurrent UTI, it would be feasible to deliver topical intravesical doses via a urinary catheter. Intravesical treatment also has the added advantage of avoiding the high systemic oral dose needed to achieve

therapeutic concentrations in the bladder lumen, which leads to side effects, and exposes both uropathogens as well as commensal bacteria in other niches to antibiotics that could exacerbate antimicrobial resistance.

Ultrasound-activated microbubbles are one attractive intracellular delivery modality solution for intracellular UTI. Gas bubbles stabilised by a polymer or surfactant coating have been in clinical use as ultrasound imaging contrast agents for over two decades [24]. Their high compressibility allows them to scatter ultrasound with a unique echo [24], and there has been considerable recent interest in their use in therapy, including permeabilisation of the blood-brain barrier [25], thermal ablation [26], and targeted delivery of drugs or genes by utilising the microbubbles as carriers [27]. Once introduced into the body, the passage of microbubbles is easily monitored via diagnostic imaging, whilst cargo delivery is achieved by applying a higher-intensity ultrasound pulse at the target location, thereby limiting side effects elsewhere. The motion of the microbubble in response to ultrasound not only releases the drug but also helps to promote its convection into the surrounding tissue and permeabilisation of cellular membranes, via a process known as “sonoporation” [28] [29]. The combination of these phenomena improves both the distribution of the drug throughout the target site, as well as its intracellular uptake. Reliable, penetrative delivery capability is particularly important in the bladder, which is lined by apical umbrella cells which elaborate protective asymmetric unit membrane plaques as well as a mucosal layer comprised of glycosaminoglycans (the so-called GAG layer) [30, 31], and may therefore be less amenable to simple lipid-based delivery systems.

The utility of microbubbles as drug delivery vehicles can be enhanced by decorating them with, for example, drug-loaded liposomes to maximize the amount of cargo that one bubble can deliver [32]. Here, we describe the development of promising ultrasound-activated gas-filled microbubbles decorated with liposomes incorporating the antibiotic gentamicin. We used a novel human bladder cell organoid model [19] infected with the uropathogen *E. faecalis*, which is common in patients with chronic infection, to assess its utility against intracellular UTI.

## Materials and methods

### Liposome Production

1,2-distearoyl-sn-glycero-3-phosphocholine (DSPC), cholesterol, 1,2-distearoyl-sn-glycero-3-phosphoethanolamine-N-[methoxy(polyethylene glycol)-2000] (ammonium salt) (DSPE-PEG(2000)), 1,2-distearoyl-sn-glycero-3-phosphoethanolamine-N-[methoxy(polyethylene glycol)-2000] – biotin (DSPE-PEG(2000)-biotin), 1,2-distearoyl-sn-glycero-3-phosphoethanolamine-N-(7-nitro-2-1,3-benzoxadiazol-4-yl) (ammonium salt) (DSPE-NBD) (Avanti Polar Lipids, Alabaster, Alabama, USA) dissolved in chloroform were combined in molar ratio of 55.5:39:2.5:2.5:0.5, at a total amount of 33 mg. The chloroform was removed and gentamicin solution (40 mg/ml) (Sigma-Aldrich) was added, followed by heating to 60°C for one hour under constant

rotation to dissolve the lipid film. The liposomes were then extruded 11 times through a 400nm membrane, followed by extrusion 11 times through a 200nm membrane at 55°C. The liposome size was then measured via dynamic light scattering [33] (Zetasizer Nano ZS, Malvern Instruments) and transferred to Phosphate Buffered Saline (PBS) (Sigma-Aldrich) via a G75 column (Sephadex G-75, Sigma-Aldrich) giving a lipid concentration of 40 mg/ml. We measured the quantity of gentamicin encapsulated in the liposomes using a previously described fluorometric o-phthaldialdehyde assay [34]. Blank control liposomes (not containing gentamicin) were produced as above but PBS was used in place of gentamicin.

### **Microbubble (bubble) production**

DSPC, DSPE-PEG(2000), DSPE-PEG(2000)-biotin, 1,2-dipalmitoyl-sn-glycero-3-phosphoethanolamine-N-(lissamine rhodamine B sulfonyl) (ammonium salt) (Rod-PE) dissolved in chloroform were added to a glass vial in a ratio of 79.5:10:10:0.5 molar percent (7 mg total). This was allowed to dry overnight to produce a lipid film. PBS (2 ml) was then added and the temperature was raised above the lipid transition temperature of DSPC (55 °C), under constant stirring for approximately 1 hour. The solution was then probe sonicated for 90 seconds to disperse the lipids using an ultrasonic cell disruptor (XL 2000, probe diameter 3 mm, Misonix Inc.) (at setting 4, for 1 minute). The headspace of the vial was then filled with Sulfur Hexafluoride (SF<sub>6</sub>, which is the main clinical contrast agent used in UK) (BOC), and the gas-liquid interface sonicated again (at setting 19, for 15 seconds) producing a white suspension. This was then centrifuged (at 300 RCF, for 10 minutes) to concentrate the microbubbles [35].

### **Binding of liposomes to bubbles**

Microbubbles were coated with liposomes as described in Lentacker *et al.* [36]. Briefly, excess avidin (Sigma Aldrich) at a concentration of 50 mg/ml (50 µl) was added to the microbubbles (500 µl) for 10 minutes followed by washing via centrifugation (300 RCF, 10 minutes). The biotin liposomes (100 µl) were then added to the microbubbles (500 µl) giving a liposome-to-microbubble lipid ratio of 4:7 mg. Liposome-coated microbubble solution was added to an improved Neubauer hemocytometer counting chamber and the number of bubbles per µl calculated using brightfield microscopy.

### **Organoid culture and infection**

The authors recently published a human bladder organoid model designed to replace the rodent model of urinary tract infection, but which is also appropriate for studying the bladder in health and disease for other indications [19]. Briefly, commercially available adult human bladder progenitor cells were grown on 12mm polycarbonate filter inserts and differentiated in the presence of sterile human urine for 14 days. Please see *Horsley et al.* [19] for further details. The organoid is long-living, urine-tolerant, fully stratified and differentiated, and highly reproducible. Expressing key biomarkers in the correct spatial compartment, it elaborates a mucus glycosaminoglycan layer

and can recapitulate several aspects of patient response to infection. The organoid was infected as previously described [19] with a clinically-relevant uropathogenic strain of *Enterococcus faecalis* which was isolated in an earlier study [18, 19].

### Ultrasound instrumentation and organoid treatment

Ultrasonic exposures were carried out using the System for Acoustic Transfection (SAT) chamber (Fig 1). This system was based on a prior design [37] with engineering modifications to allow for a decrease in the exposure area for 3D bladder organoids, because the organoids have a smaller surface area than previously used targets.

Cells and treatment agents (e.g. microbubbles, liposomes) were contained in a “sonolid” assembly, consisting of a cell culture dish ( $\mu$ -Dish 35 mm, Ibidi) friction fit to a PDMS lid fabricated by replica moulding (Sylgard 184, Dow Corning). Details of the construction and assembly are the same as in Carugo *et al.* [37] except that for the present work, an inverted 3D culture insert was fixed between the cell culture dish and the “sonolid”. The lid was sealed onto the dish ensuring no air pockets within the cell culture insert. Once the treatment agents had been added to the assembly, they were exposed to ultrasound immediately for 20 seconds. No pre-ultrasound incubation was undertaken.

The “sonolid” was held in the SAT by a circular bracket in the pre-focal region of a 40 mm radius, 120 mm radius of curvature, 1.1 MHz center frequency ultrasound transducer (Sonic Concepts, Inc. Bothell), such that the incident pressure field was focused on the cell filter insert. The transducer drive signal path consisted of a waveform generator (33220A, Agilent Technologies), low-pass filter (BLP-1.9+, Mini-Circuits), and power amplifier (A300, E&I Ltd.).

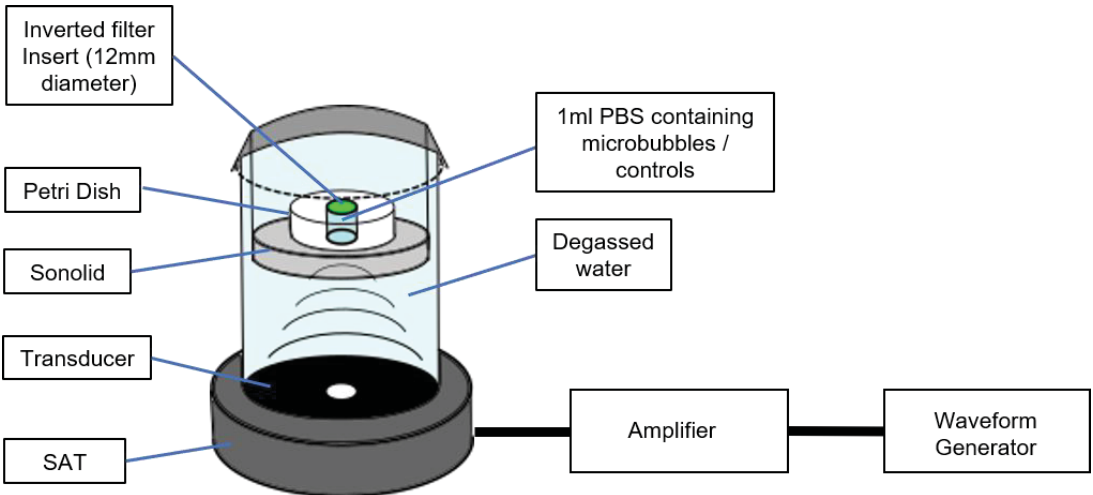


**Figure 1. System for Acoustic Transfection (SAT).** Schematic of the experimental ultrasound system used in this study.

### Ultrasound exposure conditions

Filter inserts, culture dishes and “sonolids” were assembled, placed in the ultrasound chamber and exposed to 1.1 MHz, 2.5 Mpa, 5500 cycles at 20 ms pulse duration of ultrasound for 20 seconds. These ultrasound conditions were kept constant throughout the experimental series. These ultrasound conditions were based on our previous work and work by other researchers demonstrating effective drug release from liposome-decorated gas microbubbles [38-40].

### **Compound-mediated lactate dehydrogenase (LDH) cytotoxicity assay**

Cell damage caused by free gentamicin and various doses of ultrasound-activated microbubbles was measured using a commercially available colorimetric LDH assay kit (Thermo Scientific). The assay procedure was carried out as previously described and as directed by the manufacturer [41-43]. The bladder organoids (N=3 per each treatment) were then exposed to 1000µl of controls (culture medium, urine, PBS alone exposed to ultrasound) or 1000µl of PBS containing: 200µg/ml gentamicin, 10-100µl of bubble suspension with ultrasound, 100µl of 10X lysis buffer (maximum LDH control), or culture medium containing 10% ultra-pure water (spontaneous LDH release). Organoids receiving ultrasound exposure were treated as above for 20 seconds. All organoids were subsequently incubated for 45 minutes at 37°C in 5% CO<sub>2</sub>. Post incubation, 50µl of medium from the apical liquid-liquid interface of each treated organoid was transferred to 3 wells of a flat-bottomed 96-well plate (Corning). 50µl of reaction buffer (lactate, NAD<sup>+</sup>, tetrazolium salt (INT) was then added to each well and gently mixed before protecting from light and incubating the plate at room temperature (RT) for 30 minutes. After this 30 minute period, the reaction was halted by adding 50µl of stop solution (0.16M sulfuric acid) to each well. To measure the quantity of LDH, the 96-well plate was read using a colorimetric spectrophotometer (Biochrom EZ Read 400) at an absorbance of 492nm (LDH) and 650nm (background). Microsoft Excel was used to subtract the instruments background reading from the LDH reading before calculating cytotoxicity in %, using the following formula:

$$\% \text{Cytotoxicity} = \frac{\text{Treatment associated LDH release} - \text{Spontaneous LDH release}}{\text{Maximum LDH activity} - \text{Spontaneous LDH release}} \times 100$$

### **Intracellular drug delivery**

Human urothelial organoids (N=3 per each treatment) were grown and differentiated for two weeks as above before being exposed to 1000µl of PBS containing: 0.2mg/ml NBD (fluorophore), 2µl NBD-labelled liposomes containing gentamicin, or 10µl bubbles coated with 2µl NBD-labelled liposomes with or without gentamicin. Organoids were then exposed or not exposed to ultrasound for 20 seconds. After washing 3 times in PBS the tissue was fixed in 4% formaldehyde in PBS overnight at 4°C. The fixed tissue was then permeabilised in 0.2% Triton-X100 in PBS for 15 minutes at RT, followed by a single wash with PBS. Cells were stained with Alexa Fluor-633-

conjugated phalloidin (0.6µg/ml), to label filamentous actin, and the DNA stain 4',6-diamidino-2-phenylindole, (DAPI, 1µg/µl) in PBS for 1 hour at RT. The dual-labelling solution was gently aspirated and the cells washed 5 times in PBS. Filters were carefully removed from the culture inserts with a scalpel before being mounted on a microscope slide in FluorSave reagent and a coverslip affixed with clear nail varnish. High-definition confocal microscope Z-stacks were taken at random areas of the organoids. The intracellular compartment of 20 umbrella cells per organoid (N=20 per Z-stack) were inspected for the presence of NBD (Ex. 488nm, Em. 536nm) using the ImageJ particle measurement tool [44]. To accurately compare the level of intracellular drug delivered by different treatments, fluorescence was expressed as corrected total cell fluorescence (CTCF) which accounts for integrated cell density (ID), surface area (SA) and background fluorescence readings (BR) [45, 46]. CTCF was calculated using the following formula in Microsoft Excel:

$$CTCF = ID \text{ of selected cell} - (SA \text{ of selected cell} \times BR)$$

CTCF values were averaged for each treatment prior to statistical analysis.

### **Microbial killing and microbial clearance assays**

Human urothelial organoids were grown (N=3 per each treatment) for 14 days as above before being experimentally infected with patient-isolated *E. faecalis* as described previously [19]. The infected organoids were then left untreated (control) or treated with either 20-200µl/ml of free gentamicin or 10-25µl/ml bubbles coated with gentamicin-containing liposomes. Free gentamicin-treated organoids were incubated for 2 hours whereas the bubble treated organoids were stimulated with ultrasound for 20 seconds only. The 2 hour incubation with free gentamicin was selected based on clinical studies using aminoglycoside bladder instillations [47]. To thoroughly study treatment efficacy, two independent experimental procedures were undertaken post infection and treatment (see a and b below).

a) Organoids were processed using a microbial killing assay, which relied on a traditional agar plate technique to enumerate live bacteria. The organoids were lysed with 1% Triton-X100 in PBS for 10 minutes at RT. The lysate was then serially diluted in PBS (neat, 1:100, 1:1000, 1:10000 by volume) and 25µl of each lysate dilution spread on a quartile of a Columbia blood agar (CBA, Oxoid) plate. Inoculated agar plates were incubated aerobically at 37°C for 24 hours, after which the colonies were counted to enumerate the colony forming units per millilitre (CFU/ml).

b) Organoids were inspected using quantitative image analysis to measure bacterial load. After washing 3 times in PBS the tissue was fixed in 4% formaldehyde in PBS overnight at 4°C. Cells were stained with DAPI at a concentration of 1µg/µl in PBS for 1 hour at RT, to label human and bacterial DNA. The DAPI solution was gently aspirated and cells washed 3 times in PBS. Filters were removed from the culture inserts with a scalpel before being mounted on a microscope slide as above. Z-stacks (Z-step of 0.3 µm) were

gathered at random regions of the organoids using confocal laser scanning microscopy. These 3D constructs were then analysed using nearest neighbour 3D connectivity analysis with ImageJ Object counter3D [44, 48]. Urothelial nuclei and bacterial DNA were differentiated from one another by adjusting the voxel-size filters from within Object counter3D [44, 48].

### **Antimicrobial susceptibility testing**

The minimum inhibitory concentration (MIC) of gentamicin activity against uropathogenic *E. faecalis* was calculated using the Etest method [49]. This work was performed by the Royal Free hospital, Hampstead Microbiology Department in accordance with the European Committee on Antimicrobial Susceptibility Testing (EUCAST) guidelines [50].

### **Imaging**

Brightfield and epi-fluorescence microscopy were conducted on an Olympus CX-41 upright microscope, and confocal laser scanning microscopy on Leica SP5 and SP2 microscopes. Super-resolution laser scanning confocal microscopy was performed on a Leica SP8 equipped with hybrid detectors and Lightning super-resolution module. Images were processed and analysed using Infinity Capture and Analyze V6.2.0, ImageJ 1.50j [44], Leica Application Suite X (LASX, version 3.5.2.18963) and Image-Pro Premier 3D (version 9.3) Software.

### **Statistical analyses**

Data were analysed using IBM SPSS Statistics version 25. Non-parametric Kruskal Wallis tests were performed throughout, due to the non-normal distribution of data. Median and 95% confidence interval (95% CI) plots were produced to allow visual detection of statistically significant differences. At least three experimental replicates were performed for statistical testing.

## **Results**

### **Bubble Characterisation**

SF<sub>6</sub>-filled bubbles consisting of biocompatible lipid shells (DSPC, DSPE-PEG, DSPE-PEG-biotin) were produced using sonication and decorated with fluorescently labeled gentamicin-containing liposomes (DSPC, DSPE-PEG, DSPE-PEG-biotin, DSPE-NBD, gentamicin) via an avidin-biotin complex. (see Fig. 2a for a schematic representation). Drug encapsulation was successful, with a concentration of 320 µg/ml gentamicin detected in the liposome solution using a fluorometric o-phthalaldehyde assay. Liposomes were bound to the bubbles at a ratio of 1:5, giving a final gentamicin concentration of 53 µg/ml in the liposome-coated bubble solution.

Visual inspection of uncoated bubbles (lacking liposomes) using brightfield microscopy showed the bubbles to be spherical in appearance, and image

analysis using the ImageJ measurement tool [44] revealed them to be homogeneous in diameter ( $5.08 \mu\text{m} \pm \text{SD of } 1.57$ ,  $N=30$ ) at a given focal plane (Fig. 2c). Epi-fluorescence (data not shown) and super resolution confocal microscopy of bubbles decorated with liposomes containing gentamicin and labelled with nitrobenzoxadiazole (NBD, fluorophore) demonstrated the expected staining at the bubble circumference (Fig. 2b,d). As with the uncoated microbubbles, the coated microbubbles appeared spherical and homogeneous in size; however, the liposome-coated bubbles were slightly larger with a diameter of  $5.79 \mu\text{m} \pm \text{SD of } 1.53$ ,  $N=30$ ) (Fig. 2b,d).

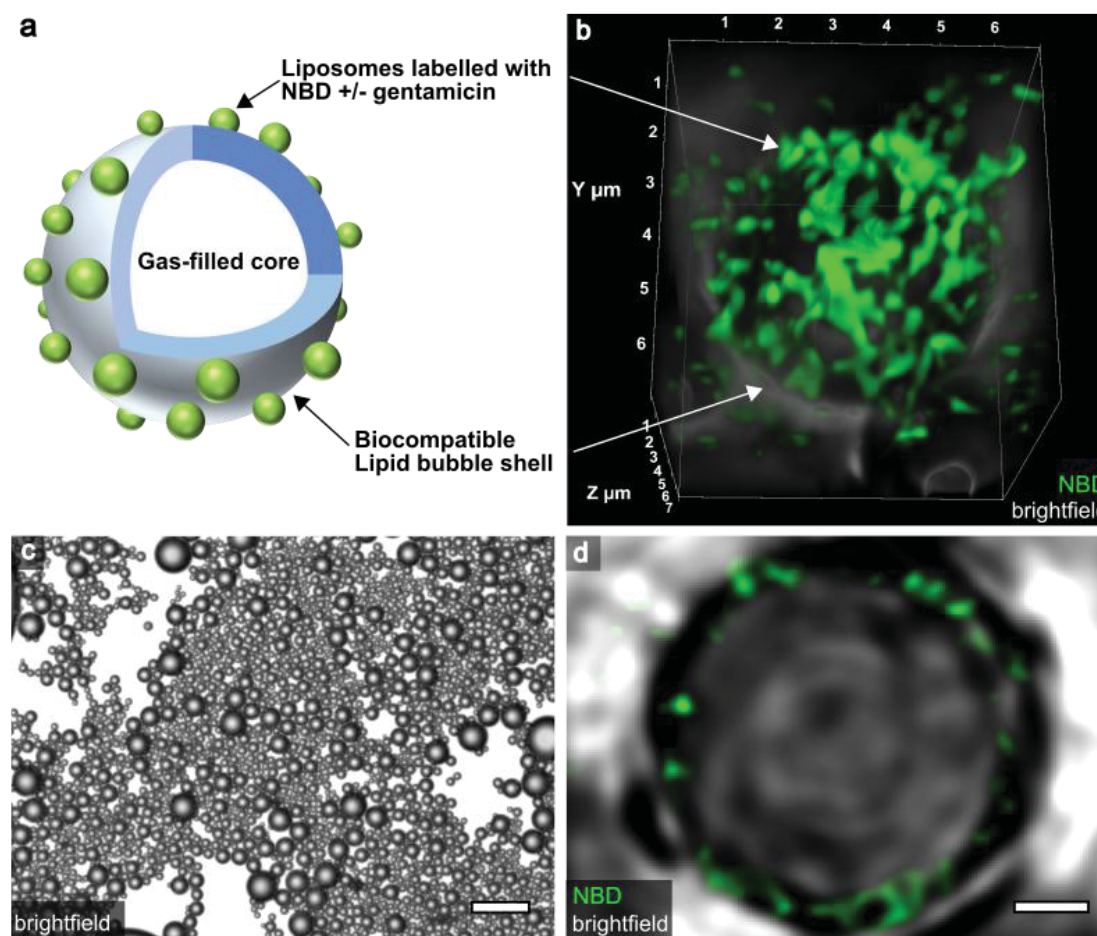


**Figure 2. Microscopic inspection and structural schematic of bubbles.**

(a) Schematic of a single liposome-decorated bubble. Bubble shells were constructed from biocompatible lipids surrounding a gaseous sulphur hexafluoride ( $\text{SF}_6$ ) core. The bubble shell is decorated with liposomes containing a fluorescent dye (NBD, nitrobenzoxadiazole) with or without gentamicin. (b) Confocal super-resolution 3D image of a single microbubble decorated with fluorescent (NBD) liposomes containing gentamicin. Each coated bubble is  $5.79 \mu\text{m} \pm \text{SD of } 1.53$  in diameter. (c) Monochrome image of uncoated bubbles taken using brightfield microscopy. Each bubble is  $5.08 \mu\text{m} \pm \text{SD of } 1.57$  in diameter when examined in the same focal plane (bubbles that appear larger are closer to the objective). Scale bar represents  $40 \mu\text{m}$ . (d) Single confocal super-resolution Z-slice (cross-section) showing fluorescent liposome binding at the bubble circumference. Scale bar represents  $1 \mu\text{m}$ .

**The cytotoxicity of low-dose ultrasound-activated bubble therapy is comparable to that of conventional antimicrobial treatment in a human urothelial organoid model**

To explore the delivery parameters of the bubbles, we used the HBLAK human urothelial organoid model. Given the significant differences between the rodent and human bladder in both ultrastructure and physiology, this organoid model can be considered to be preferable in some respects to live rodent models of epithelial biology and infection [19]. The HBLAK organoid model has also been shown to have structural, morphological and biomarker-expression similarities to the human urothelium, and to offer a viable platform for studying urinary tract infection [19]. In the first set of experiments we challenged three-dimensionally differentiated mature, fully stratified and differentiated organoids with controls, a therapeutic dose of gentamicin and a range of bubble concentrations stimulated with ultrasound. The quantity of released lactate dehydrogenase (LDH) was then detected using a colorimetric LDH assay to explore and compare the levels of cytotoxicity induced by these differing treatments and dosages.

Firstly, to standardise bubble treatment dosages, the freshly prepared bubble solution was added to a haemocytometer to count the number of intact bubbles per  $\mu\text{l}$ . This procedure was repeated prior to all subsequent experimentation to ensure repeatability. As expected, the addition of culture medium to the human urothelial organoid resulted in no cytotoxicity ( $n=3$ ) (Fig. 3). Moreover, supporting the urine-dependant nature of the urothelial organoid [19], human urine also resulted in no cell damage ( $n=3$ ). Additionally, toxicity caused by ultrasound exposure alone was negligible ( $n=3$ ) (Med=0.23%, 95% CI: .235, .618). Exposure of urothelial organoids to 200  $\mu\text{g/ml}$  of free gentamicin solution (comparable to human urinary concentrations post intramuscular gentamicin treatment for UTI [51]) had a median cytotoxic effect of 11.61% (95% CI: 10.597, 13.628) ( $n=3$ ).

Cytotoxicity induced by ultrasound-activated bubbles, coated with blank or gentamicin-containing liposomes, increased in a dose-responsive manner (Fig. 3). However, bubbles decorated with gentamicin-containing liposomes appeared to be more toxic than those decorated with blank liposomes, particularly at higher doses. For example, treatment with 10  $\mu\text{l}$  of bubble solution, containing blank or gentamicin liposomes, caused a median of 13.51% (95% CI: 13.275, 14.747) ( $n=3$ ) and 13.65% (95% CI: 13.481, 14.158) ( $n=3$ ) cell disruption, respectively. In contrast, 100  $\mu\text{l}$  of blank bubble solution induced a median of 26.58% (95% CI: 26.109, 28.375) ( $n=3$ ) cell death whereas 100  $\mu\text{l}$  of their gentamicin-containing counterparts caused 36.35% (95% CI: 35.616, 39.031) ( $n=3$ ) (Fig. 3). A Kruskal-Wallis test confirmed that a highly statistically significant difference existed between the level of toxicity induced by the various treatments and doses  $\chi^2(11)=36.47$ ,  $p<.001$  (Fig. 3).

Visual inspection of the median and 95% CI plot generated from these data highlighted two distinct clusters where there appeared to be significant data

overlap. A 'lower' cluster generated by the median (%) toxicity caused by free-gentamicin, 10 µl bubble dose and 25 µl bubble dose, and an 'upper' cluster caused by the 50 µl and 100 µl bubble doses (Fig. 3).

In summary, low-dose ultrasound-activated bubble therapy exhibits a comparable level of cytotoxicity to that of conventional gentamicin treatment in a human urothelial model. Higher doses (50 and 100 µl) of the bubble preparation, at least in this model system, resulted in increased levels of cell death. Therefore, we decided to exclude the higher doses in subsequent experiments.

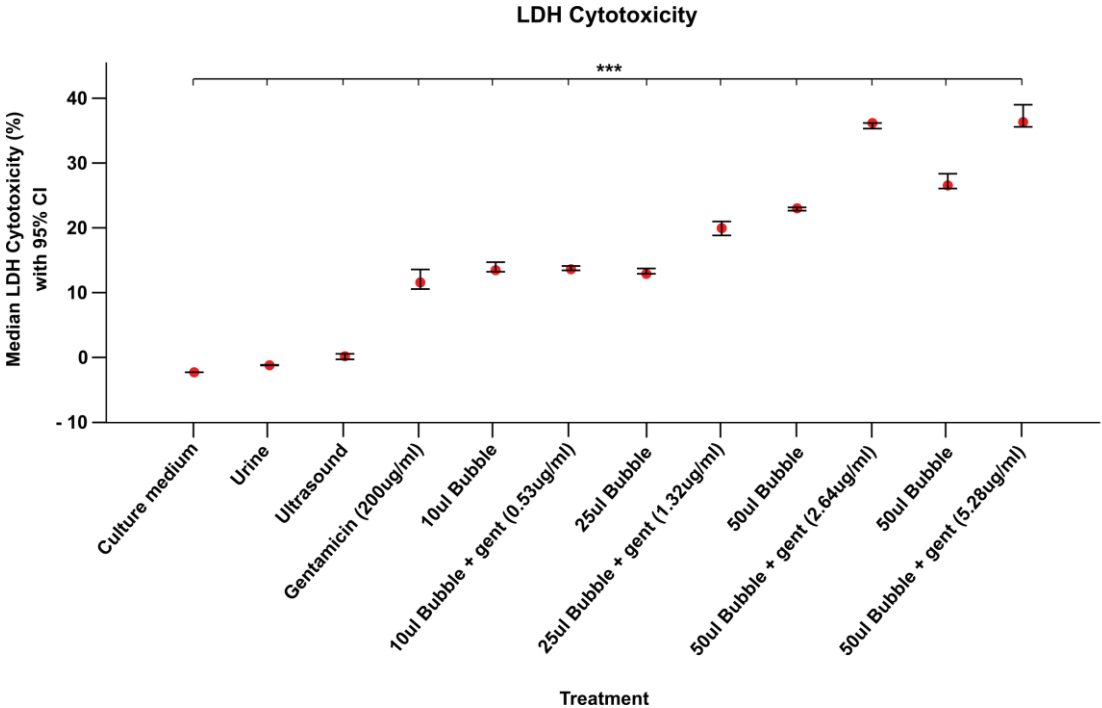


**Figure 3. The cytotoxicity of low-dose ultrasound-activated bubble therapy is comparable to that of conventional antimicrobial treatment in a human urothelial organoid model.** Human urothelial organoids were exposed to ultrasound alone, control substances, free gentamicin or a range of bubble doses activated with ultrasound. Bubbles were coated with blank liposomes or liposomes containing gentamicin. Cytotoxicity was calculated by measuring LDH release using a colorimetric assay. All experiments were repeated in triplicate. Median and 95% CI plot showing the degree of cytotoxicity (%) induced by control substances and increasing quantities of ultrasound-activated bubbles with or without gentamicin. Control substances and ultrasound alone caused no cell damage whereas cytotoxicity due to free gentamicin and ultrasound-activated bubbles increased in a dose-dependent manner. N=3 per treatment. Abbreviations; gent (gentamicin), LDH (lactate dehydrogenase). \*\*\*P<.001.

**Ultrasound-activated bubbles exhibit significantly higher intracellular delivery than do liposomes alone**

We explored the ability of liposomes and liposome-decorated bubbles to deliver a fluorescent compound into the intracellular compartment of human urothelial cells of the organoid model in the presence of ultrasound. Mature, three-dimensionally differentiated and stratified organoids were exposed to NBD alone, 2µl NBD-labelled liposomes containing gentamicin; or 10µl bubbles coated with 2µl NBD-labelled liposomes with or without gentamicin. Half of the organoids were exposed to ultrasound for 20 seconds and the remainder left untreated. Post treatment, the organoids were stained and imaged using confocal microscopy to determine and compare the level of intracellular NBD using corrected total cellular fluorescence (CTCF) (Fig 4a).

Treatment with NBD solution alone (n=3) resulted in a median intracellular CTCF value of 425.66 (95% CI: 328.859, 1624.013) (Fig 4b). Liposomes without ultrasound stimulation (n=3) readily delivered NBD into the apical umbrella cells of the organoid (Med=3533.57, 95% CI: 2161.869, 5170.675), however, acoustic stimulation (n=3), judging by the 95% confidence intervals, appeared to have no statistically significant influence (Med=4100.16, 95% CI: 3530.942, 4197.943) (Fig 4b).

Intracellular NBD delivery via the blank-liposome-coated bubbles without ultrasound (n=3) was similar to liposomes alone (Med=4553.93, 95% CI: 4250.599, 6339.808). That said, when stimulated with ultrasound (n=3), the intracellular NBD CTCF value increased by a factor of two (Med=9544.68, 95% CI: 4555.101, 11293.254) (Fig 4b). Bubbles decorated with gentamicin containing liposomes, in the absence of ultrasound (n=3), appeared to deliver a relatively low concentration of NBD (Med=427.34, 95% CI: 381.311, 4241.87) (Fig 4b). However, as with the bubbles coated with blank liposomes, the intracellular CTCF increased dramatically under acoustic stimulation (n=3) (Med=7132.13, 95% CI: 6418.691, 11316.31) (Fig 4b). The result of a Kruskal-Wallis test showed there to be a statistically significant difference between the intracellular NBD CTCF values delivered by these various treatment modalities  $\chi^2(6)=16.364$ ,  $p=.012$  (Fig 4b).

Taken together, these results show that ultrasound-activated liposome-coated bubbles can efficiently deliver high concentrations of compounds into the intracellular compartment of human urothelial cells. Moreover, they were able to deliver twice the concentrations than liposomes alone and over 16 times the concentrations achieved by NBD via free diffusion.

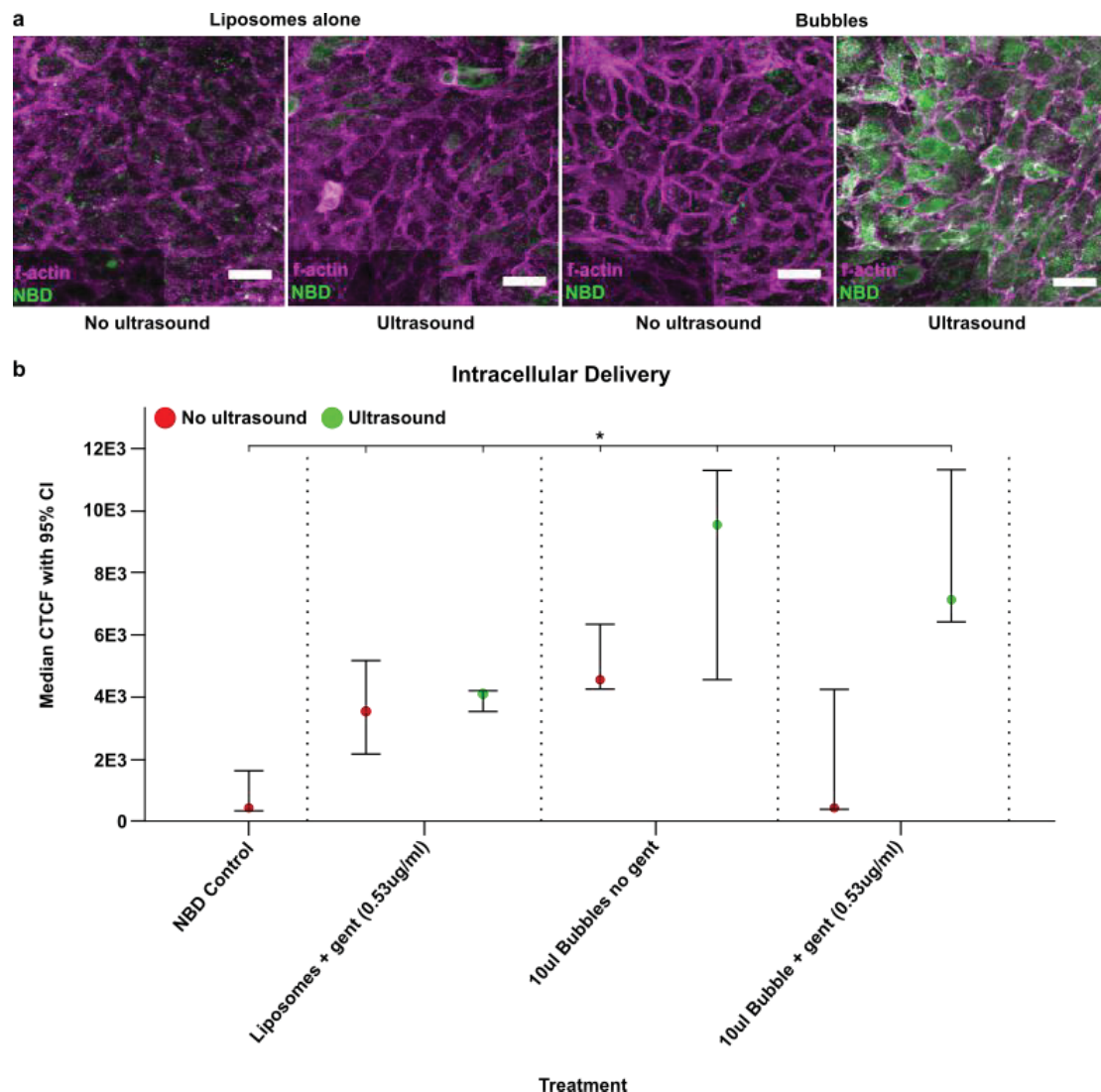


**Figure 4. Ultrasound-activated bubbles exhibit significantly higher intracellular delivery than do liposomes alone.** Human urothelial organoids were exposed to NBD (fluorophore) in solution, NBD-labelled liposomes containing gentamicin, or bubbles coated with NBD-labelled liposomes with or without gentamicin. After exposure to ultrasound or no exposure to ultrasound, treated organoids were fixed. High-definition laser scanning confocal z-stacks of each organoid were analysed to measure intracellular delivery using corrected total cellular fluorescence (CTCF). All experiments were repeated in triplicate. (a) Representative intracellular confocal slices within the umbrella cell layer of human organoid after liposome or bubble treatment with or without ultrasound. Phalloidin labelled f-actin is shown in magenta and intracellular NBD is shown in green. Scale bars represent 40µm. (b) Median and 95% CI plot comparing intracellular drug delivery of each treatment with or without the addition of gentamicin and acoustic stimulation (see colour coded key). N=3 per treatment. Abbreviations; Bub (bubbles), Lip (liposomes), gent (gentamicin), NBD (nitrobenzoxadiazole). \*P<.05.

**Ultrasound-activated bubble therapy is effective at killing and clearing uropathogenic *E. faecalis* in a human model of UTI**

*Enterococcus faecalis* is responsible for a significant proportion of chronic UTI cases [18], likely due in part to its ability to invade the cells of the urothelium [18, 19]. We previously showed in the HBLAK organoid model that *E. faecalis* invades the apical urothelium to establish intracellular reservoirs similar to those previously seen in urothelial cells shed from patients with UTI [18], making this infection model an excellent test-bed for trialling therapies designed to eradicate intracellular infection.

In the next set of experiments, we infected human urothelial organoids with a patient-isolated strain of *E. faecalis* before treating them with either free gentamicin for 2 hours or ultrasound-activated bubble (coated with gentamicin containing liposomes) therapy for 20 seconds. Post treatment, the organoid cultures were lysed with detergent and the lysate plated on microbiological agar to measure the quantity of live bacteria.

The lysate harvested from untreated organoids (n=6) grew a median of  $3 \times 10^7$  colony-forming units (CFU)/ml (95% CI:  $2 \times 10^7$ ,  $3.2 \times 10^7$ ) (Fig 5a). The number of live *E. faecalis* after treatment for 2 hours with 20 µg/ml of free gentamicin (n=3) was lower than in the untreated organoid, if not substantially (Med= $2.28 \times 10^7$ , 95% CI:  $1.66 \times 10^7$ ,  $2.4 \times 10^7$ ) (Fig 5a). The results of antimicrobial susceptibility testing showed growth of this strain of *E. faecalis* to be inhibited by 7 µg/ml of gentamicin. Unsurprisingly, therefore, the addition of 200 µg/ml (n=3) was far more potent (Med= $1.96 \times 10^6$ , 95% CI:  $9.12 \times 10^6$ ,  $4.4 \times 10^6$ ) (Fig 5a). Interestingly the 10 µl and 25 µl acoustically-stimulated microbubble doses resulted in substantial bacterial death (Med= $8 \times 10^6$ , 95% CI:  $1.4 \times 10^6$ ,  $8.4 \times 10^6$  and Med= $8 \times 10^6$ , 95% CI:  $1.6 \times 10^6$ ,  $1 \times 10^7$  respectively) (Fig 5a). This is a remarkable and less expected result given the far lower gentamicin concentrations found in the microbubble preparations (0.53 µg/ml in 10 µl and 1.32 µg/ml in 25 µl). The result of a Kruskal-Wallis test showed there to be a statistically significant difference between the number of *E. faecalis* killed by these treatments  $\chi^2(4)=15.499$ , p=.004 (Fig 5a).

In addition to the microbiological methods deployed above, we also analysed infected organoids using an imaging technique to ascertain the level of bacterial burden pre- and post-treatment. To achieve this, a further set of human urothelial organoids were grown, infected and treated as above but, in contrast to the last experiments, they were then fixed and stained in preparation for confocal microscopy. High resolution Z-stacks were acquired (Fig. 6b) at random fields before analysing these 3D constructs using a 3D nearest neighbour connectivity technique [48] to enumerate the number of *E. faecalis* per human cell.

The untreated organoids (n=3) contained a median of 34.17 (95% CI: 23.54, 43.54) bacteria per urothelial cell (Fig. 5c). Two hours of exposure to either 20 µl/ml (n=3) or 200 µl/ml (n=3) of free gentamicin appeared to have little effect on bacterial burden (Med=43.07, 95% CI: 35.53, 47.92 and Med=36.15, 95% CI: 30.97, 46.41 respectively) (Fig. 5c). In contrast, however, the 10 µl dose (n=3) of ultrasound-activated bubble treatment dramatically lowered the bacterial load in this system (Med=12.61, 95% CI: 9.69, 26.46) (Fig. 5c). Furthermore, bacterial burden in the infected urothelial organoids treated with

the higher bubble dose (25  $\mu$ l) (n=3) appeared lower still (Med=9.11, 95% CI: 7.07, 10.33) (Fig. 5c). The result of a Kruskal-Wallis test showed there to be a statistically significant difference between the number of *E. faecalis* per urothelial cell after each of these treatments  $\chi^2(4)=10.6$ , p=.031 (Fig. 5c).

Taken together, our data show that acoustically stimulated bubble therapy is promising in its ability to kill and remove uropathogenic *E. faecalis* embedded in a human urothelial organoid. Moreover, these results were achieved within 20 seconds by sub-clinical concentrations of encapsulated gentamicin.

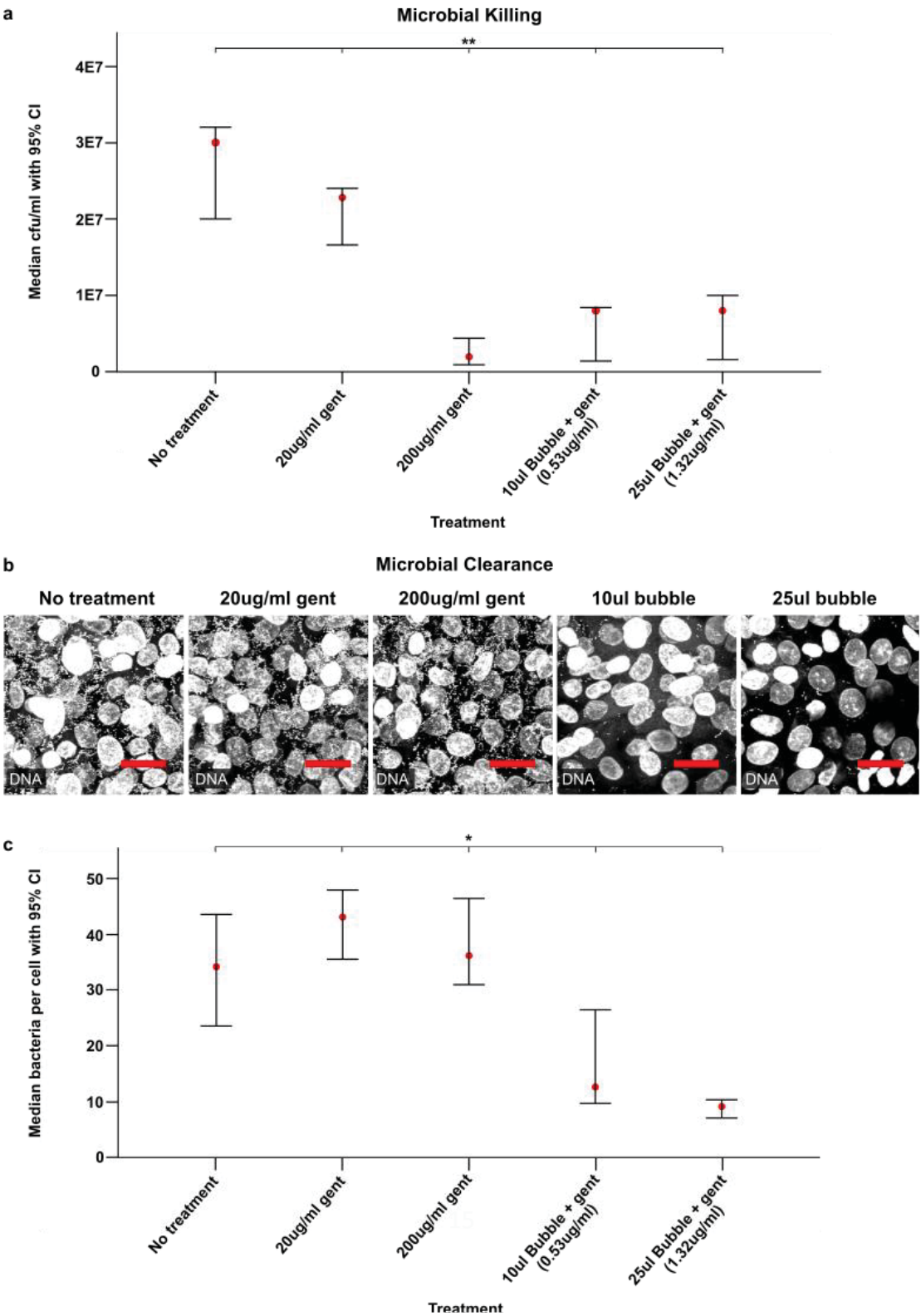


**Figure 5. Ultrasound-activated bubble therapy is effective at killing and clearing uropathogenic *E. faecalis* in a human model of UTI .** Human urothelial organoids were infected with patient-isolated *E. faecalis* before being treated with either free gentamicin or bubbles coated with gentamicin-containing liposomes. Free gentamicin-treated organoids were incubated for 2 hours whereas the bubble treated organoids were stimulated with ultrasound for 20 seconds only. Post treatment the organoids were either: 1) lysed with detergent and the lysate added to agar plates to enumerate the bacterial colony forming units per millilitre (CFU/ml) or; 2) stained, imaged and analysed to enumerate the number of bacteria per urothelial cell, thus investigating levels of bacterial clearance. All experiments were repeated in triplicate. (a) Median and 95% CI plot presenting the number of live bacteria detected after no treatment (N=3), free gentamicin treatment (N=3 at each dose) and ultrasound-activated bubble therapy (N=3 at each dose). (b) Representative maximum projection confocal images of infected human urothelial organoids post treatment. Host (urothelial nuclei, larger circular structures) and bacterial (*E. faecalis*, small circular specks) DNA were labelled with DAPI. Scale bars represent 20µm. (c) Median and 95% CI plot comparing the number of bacteria adhered to each urothelial cell after no treatment (N=3), free gentamicin (N=3 for each dose) and ultrasound-activated bubble treatment (N=3 for each dose). Abbreviations; gent (gentamicin). \*P<.05, \*\*P<.01.

In summary, this mode of treatment was able to concentrate drug in the intracellular space of these highly specialised cells. Furthermore, acoustically-stimulated bubble treatment shows promise as a safe, fast and effective modality in regards to both killing and removal of uropathogenic *E. faecalis* in a human-derived bladder organoid.

## Discussion

UTIs frequently reoccur and current oral antibiotic regimens fail in a high percentage of cases [15, 52]. Moreover, the use of antibiotics can cause a number of systemic side effects and is linked to a worrying increase in worldwide antibiotic resistance [8, 11, 53]. In an effort to avoid these problems, some clinics advocate the use of gentamicin bladder irrigations; however, these appear to share a similar failure rate to that of oral administration [54]. More recently, novel nanotechnology-driven drug delivery systems have been gaining attention in this research arena [55]. Indeed, the use of liposome-coated microbubbles stimulated with ultrasound are showing promise in a number of disciplines [38, 39, 56].

Until now, however, this technology had not been translated for drug delivery in the bladder. We decided to explore the potential for ultrasound-activated microbubble drug delivery as an alternative intravesical treatment for UTI. Using our characterised human urothelial organoid as an *in vitro* test-bed, we showed that microbubble therapy safely delivered drug into the intracellular space of highly-specialised umbrella cells. Furthermore, in this human model of UTI, our delivery system was effective at both killing and clearing

uropathogenic *E. faecalis*, which is very common amongst chronically infected patients [18, 57-59]. It should be relatively straightforward to translate this delivery system to the outpatient clinical setting, with delivery via a simple urinary catheter, followed by ultrasound-guided treatment, similar in spirit to lithotripsy currently used to eradicate kidney stones. Moreover, the compounds making up the delivery system are already approved for clinical use as contrast agents, which could streamline their regulatory approval [60, 61]. In future preclinical and clinical trials, it should be possible to determine the optimal regimen (dose and number of administrations) needed to eradicate a deeply entrenched chronic infection. Gentamicin bladder instillations, which frequently fail, are usually administered twice a day for several weeks [54]. It is our hope, using this technology, that we should be able to drastically shorten treatment times. From a practical point of view, it should be noted that the amount of bubbles present in the overall volume of PBS in the test chamber (25  $\mu$ l bubbles: 1000  $\mu$ l PBS) can be scaled up for clinical use easily, as intravesical volumes tend to be approximately 100 ml; therefore the addition of 2.5 ml of bubbles would achieve the desired 1:40 dilution. As regards safety, our LDH experiments are reassuring, but we acknowledge that the effects of cavitation on tissue integrity will need to be assessed in future studies.

In this therapeutic strategy, the bubbles bring the liposomes to the cell surface and propel the liposomes into the cells during ultrasound exposure [36, 62, 63]. The ultrasound-activated bubbles were able to deliver nearly twice the concentration of drug into the organoid umbrella cells than could liposomes alone. Considering the efficiency of liposomal drug delivery for the treatment of other pathologies, this is a promising result [64]. Moreover, ultrasound had a highly significant effect on drug delivery by the bubbles, demonstrating activation and hence presumably cavitation in response to the acoustic field. In future, it would be of interest to identify the specific intracellular compartments that receive 'payload' during ultrasound-mediated microbubble delivery. A number of endocytic pathways have been implicated in the trafficking of therapeutic nanoparticles [1]. Due to the mechanical activity of sonoporation, however, it would seem likely that delivery is achieved via direct membrane penetration (translocation) into the cytosol proper [1]; there are reports of intact 2  $\mu$ m bubbles entering cells and numerous reports for liposomes [36]. Although it might be possible to streamline the regulatory approval for this approach by simply co-administering clinically approved microbubbles with free gentamicin, it is known that conjugation greatly improves delivery [38][65].

Of note, the concentration of gentamicin encapsulated in the liposomes coating the microbubbles was far lower than the reported minimum inhibitory concentration value for this uropathogen. It is possible, therefore, that this highly enhanced bactericidal activity is a result of a propensity of this delivery system to concentrate drug in the intracellular space of infected cells. In this case, gentamicin levels could be in excess of the aforementioned MIC value within the bacterial niche. Future work is required to understand and tailor this novel treatment modality to the pathophysiology of the system. In addition, once more is understood about how *E. faecalis* and other uropathogens gain

access to the intracellular space, ligands could be easily added to the microbubble / liposome shells to provide targeted delivery as a further improvement [66].

In line with the encouraging intracellular delivery data, ultrasound-activated bubble therapy was effective at killing and clearing *E. faecalis* from a human urothelial organoid. A cytotoxicity assay showed that the low-dose ultrasound-activated bubble therapy which translated into efficient bacterial killing was no more harmful than 200 µg/ml of free gentamicin solution – a level already approved for clinical use. A 20-second exposure to this novel therapy was as potent as 2 hours of 200 µg/ml free gentamicin at killing *E. faecalis*. Moreover, ultrasound-activated bubble therapy resulted in a ~75% reduction in bacterial burden when compared with free gentamicin treatment. It must be noted that microbubble treatment may be removing a proportion of live bacteria from the organoid which were subsequently lost during the staining procedure; conversely the free gentamicin treatment may kill bacteria but leave them physiologically attached. This fact would account for the interesting discrepancies between our bacterial killing and clearance assays. Even so, *in vivo*, a 100% bacterial kill would not be likely, nor necessary, as the de-adhered live bacteria would be excreted during urination. Patients suffering from UTI may find it difficult to tolerate long exposure times during administration of intravesical drugs. A recent study reported only half of participants suffering from recurrent UTI were able to tolerate a 30-minute installation of Cystistat™ [67]. Therefore, shorter treatment times may confer an advantage in the clinical setting.

In summary, new treatments for UTI are urgently needed and this proof-of-concept data suggest that ultrasound-activated microbubbles could be highly efficacious whilst potentially avoiding the common drawbacks of systemic treatment in a vulnerable population. This modality might also find utility in other chronic infection systems where entrenched bacteria are difficult to clear, and, further afield, could be of use for any indication where robust intracellular delivery is required.

## Conflict of interest

The authors confirm that there are no known conflicts of interest associated with this publication and there has been no significant financial support for this work that could have influenced its outcome.

## Acknowledgements

We would like to thank the Multiple Sclerosis Society for their generous financial support of this work (grant reference 986)

## References

- 767 1. Garnacho, C., *Intracellular Drug Delivery: Mechanisms for Cell Entry*. Curr  
768 Pharm Des, 2016. **22**(9): p. 1210-26.
- 769 2. Kamaruzzaman, N.F., S. Kendall, and L. Good, *Targeting the hard to reach:  
770 challenges and novel strategies in the treatment of intracellular bacterial  
771 infections*. 2017. **174**(14): p. 2225-2236.
- 772 3. Bjarnsholt, T., *The role of bacterial biofilms in chronic infections*. APMIS, 2013.  
773 **121**(s136): p. 1-58.
- 774 4. Foxman, B., *Epidemiology of urinary tract infections: incidence, morbidity,  
775 and economic costs*. Am J Med, 2002. **113 Suppl 1A**: p. 5S-13S.
- 776 5. Christian, R., *Do prophylactic antibiotics reduce UTI risk after urodynamic  
777 studies?* Am J Nurs, 2014. **114**(2): p. 20.
- 778 6. Foxman, B., *The epidemiology of urinary tract infection*. Nat Rev Urol, 2010.  
779 **7**(12): p. 653-60.
- 780 7. Córdoba, G., et al., *Use of diagnostic tests and the appropriateness of the  
781 treatment decision in patients with suspected urinary tract infection in  
782 primary care in Denmark – observational study*. BMC Family Practice, 2018.  
783 **19**: p. 65.
- 784 8. (WHO), W.H.O., *Antimicrobial resistance. Fact sheet 194*. 2014.
- 785 9. Khasriya, R., et al., *Spectrum of bacterial colonization associated with  
786 urothelial cells from patients with chronic lower urinary tract symptoms*. J Clin  
787 Microbiol, 2013. **51**(7): p. 2054-62.
- 788 10. Pearce, M.M., et al., *The female urinary microbiome: a comparison of women  
789 with and without urgency urinary incontinence*. MBio, 2014. **5**(4): p. e01283-  
790 14.
- 791 11. Swamy, S., et al., *Recalcitrant chronic bladder pain and recurrent cystitis but  
792 negative urinalysis – What should we do? . International Urogynecology  
793 Journal; Accepted manuscript*, 2018.
- 794 12. Foxman, B., *Epidemiology of urinary tract infections: incidence, morbidity,  
795 and economic costs*. Dis Mon, 2003. **49**(2): p. 53-70.
- 796 13. Michaud, J.E., et al., *Cytotoxic Necrotizing Factor-1 (CNF1) does not promote  
797 E. coli infection in a murine model of ascending pyelonephritis*. BMC  
798 Microbiology, 2017. **17**: p. 127.
- 799 14. Peach, B.C., et al., *Risk Factors for Urosepsis in Older Adults: A Systematic  
800 Review*. Gerontology and geriatric medicine, 2016. **2**: p. 2333721416638980.
- 801 15. Hunstad, D.A. and S.S. Justice, *Intracellular lifestyles and immune evasion  
802 strategies of uropathogenic Escherichia coli*. Annu Rev Microbiol, 2010. **64**: p.  
803 203-21.
- 804 16. Anderson, G.G., et al., *Intracellular bacterial biofilm-like pods in urinary tract  
805 infections*. Science, 2003. **301**(5629): p. 105-7.
- 806 17. Eto, D.S., J.L. Sundsbak, and M.A. Mulvey, *Actin-gated intracellular growth  
807 and resurgence of uropathogenic Escherichia coli*. Cell Microbiol, 2006. **8**(4):  
808 p. 704-17.
- 809 18. Horsley, H., et al., *Enterococcus faecalis subverts and invades the host  
810 urothelium in patients with chronic urinary tract infection*. PLoS One, 2013.  
811 **8**(12): p. e83637.

- 812 19. Horsley, H., et al., *A urine-dependent human urothelial organoid offers a*  
813 *potential alternative to rodent models of infection*. Scientific Reports, 2018.  
814 **8**(1): p. 1238.
- 815 20. Szabados, F., et al., *Staphylococcus saprophyticus ATCC 15305 is internalized*  
816 *into human urinary bladder carcinoma cell line 5637*. Fems Microbiology  
817 Letters, 2008. **285**(2): p. 163-169.
- 818 21. Rosen, D.A., et al., *Utilization of an intracellular bacterial community pathway*  
819 *in Klebsiella pneumoniae urinary tract infection and the effects of FimK on*  
820 *type 1 pilus expression*. Infect Immun, 2008. **76**(7): p. 3337-45.
- 821 22. Darouiche, R.O. and R.J. Hamill, *Antibiotic penetration of and bactericidal*  
822 *activity within endothelial cells*. Antimicrob Agents Chemother, 1994. **38**(5):  
823 p. 1059-64.
- 824 23. Langer, R., *Drug delivery and targeting*. Nature, 1998. **392**(6679 Suppl): p. 5-  
825 10.
- 826 24. Cosgrove, D., *Ultrasound contrast agents: an overview*. Eur J Radiol, 2006.  
827 **60**(3): p. 324-30.
- 828 25. Meairs, S. and A. Alonso, *Ultrasound, microbubbles and the blood-brain*  
829 *barrier*. Progress in Biophysics & Molecular Biology, 2007. **93**(1-3): p. 354-  
830 362.
- 831 26. Luo, W., et al., *Enhancing effects of SonoVue, a microbubble sonographic*  
832 *contrast agent, on high-intensity focused ultrasound ablation in rabbit livers*  
833 *in vivo*. Journal of Ultrasound in Medicine, 2007. **26**(4): p. 469-476.
- 834 27. Bull, J.L., *The application of microbubbles for targeted drug delivery*. Expert  
835 Opinion on Drug Delivery, 2007. **4**(5): p. 475-493.
- 836 28. Bazan-Peregrino, M., et al., *Ultrasound-induced cavitation enhances the*  
837 *delivery and therapeutic efficacy of an oncolytic virus in an in vitro model*. J  
838 Control Release, 2012. **157**(2): p. 235-42.
- 839 29. Lentacker, I., et al., *Understanding ultrasound induced sonoporation:*  
840 *Definitions and underlying mechanisms*. Adv Drug Deliv Rev, 2013.
- 841 30. Wu, X.R., et al., *Uroplakins in urothelial biology, function, and disease*. Kidney  
842 Int, 2009. **75**(11): p. 1153-65.
- 843 31. Nordling, J. and A. van Ophoven, *Intravesical glycosaminoglycan*  
844 *replenishment with chondroitin sulphate in chronic forms of cystitis. A multi-*  
845 *national, multi-centre, prospective observational clinical trial*.  
846 Arzneimittelforschung, 2008. **58**(7): p. 328-35.
- 847 32. Geers, B., et al., *Ultrasound responsive doxorubicin-loaded microbubbles;*  
848 *towards an easy applicable drug delivery platform*. J Control Release, 2010.  
849 **148**(1): p. e59-60.
- 850 33. Matsuzaki, K., et al., *Optical characterization of liposomes by right angle light*  
851 *scattering and turbidity measurement*. Biochimica et Biophysica Acta (BBA) -  
852 Biomembranes, 2000. **1467**(1): p. 219-226.
- 853 34. Gubernator, J., Z. Drulis-Kawa, and A. Kozubek, *A simply and sensitive*  
854 *fluorometric method for determination of gentamicin in liposomal*  
855 *suspensions*. Int J Pharm, 2006. **327**(1-2): p. 104-9.
- 856 35. Feshitan, J.A., et al., *Microbubble size isolation by differential centrifugation*.  
857 Journal of Colloid and Interface Science, 2009. **329**(2): p. 316-324.

36. Lentacker, I., et al., *Lipoplex-Loaded Microbubbles for Gene Delivery: A Trojan Horse Controlled by Ultrasound*. Advanced Functional Materials, 2007. **17**(12): p. 1910-1916.
37. Carugo, D., et al., *Biologically and Acoustically Compatible Chamber for Studying Ultrasound-Mediated Delivery of Therapeutic Compounds*. Ultrasound in Medicine and Biology, 2015.
38. Geers, B., et al., *Self-assembled liposome-loaded microbubbles: The missing link for safe and efficient ultrasound triggered drug-delivery*. J Control Release, 2011. **152**(2): p. 249-56.
39. Escoffre, J.M., et al., *Doxorubicin liposome-loaded microbubbles for contrast imaging and ultrasound-triggered drug delivery*. IEEE Trans Ultrason Ferroelectr Freq Control, 2013. **60**(1): p. 78-87.
40. Cool, S.K., et al., *Coupling of drug containing liposomes to microbubbles improves ultrasound triggered drug delivery in mice*. Journal of Controlled Release, 2013. **172**(3): p. 885-893.
41. Nachlas, M.M., et al., *The determination of lactic dehydrogenase with a tetrazolium salt*. Analytical Biochemistry, 1960. **1**(4): p. 317-326.
42. Korzeniewski, C. and D.M. Callewaert, *An enzyme-release assay for natural cytotoxicity*. J Immunol Methods, 1983. **64**(3): p. 313-20.
43. Decker, T. and M.-L. Lohmann-Matthes, *A quick and simple method for the quantitation of lactate dehydrogenase release in measurements of cellular cytotoxicity and tumor necrosis factor (TNF) activity*. Journal of Immunological Methods, 1988. **115**(1): p. 61-69.
44. Schneider, C.A., W.S. Rasband, and K.W. Eliceiri, *NIH Image to ImageJ: 25 years of image analysis*. Nat Meth, 2012. **9**(7): p. 671-675.
45. Burgess, A., et al., *Loss of human Greatwall results in G2 arrest and multiple mitotic defects due to deregulation of the cyclin B-Cdc2/PP2A balance*. Proc Natl Acad Sci U S A, 2010. **107**(28): p. 12564-9.
46. McCloy, R.A., et al., *Partial inhibition of Cdk1 in G 2 phase overrides the SAC and decouples mitotic events*. Cell Cycle, 2014. **13**(9): p. 1400-12.
47. Huynh, D. and J.A. Morgan, *Use of intravesicular amikacin irrigations for the treatment and prophylaxis of urinary tract infections in a patient with spina bifida and neurogenic bladder: a case report*. The journal of pediatric pharmacology and therapeutics : JPPT : the official journal of PPAG, 2011. **16**(2): p. 102-107.
48. Bolte, S. and F.P. Cordelières, *A guided tour into subcellular colocalization analysis in light microscopy*. Journal of Microscopy, 2006. **224**(3): p. 213-232.
49. Nachnani, S., et al., *E-test: a new technique for antimicrobial susceptibility testing for periodontal microorganisms*. J Periodontol, 1992. **63**(7): p. 576-83.
50. *EUCAST: AST of bacteria*. 2017 21/07/2017]; Available from: [http://www.eucast.org/ast\\_of\\_bacteria/](http://www.eucast.org/ast_of_bacteria/).
51. Labovitz, E., M.E. Levison, and D. Kaye, *Single-Dose Daily Gentamicin Therapy in Urinary Tract Infection*. Antimicrobial Agents and Chemotherapy, 1974. **6**(4): p. 465-470.
52. Milo, G., et al., *Duration of antibacterial treatment for uncomplicated urinary tract infection in women*. Cochrane Database Syst Rev, 2005(2): p. Cd004682.

- 904 53. Wagenlehner, F.M., et al., *[Antibiotic resistance and their significance in*  
905 *urogenital infections: new aspects]*. Urologe A, 2014. **53**(10): p. 1452-7.
- 906 54. Defoor, W., et al., *Safety of gentamicin bladder irrigations in complex*  
907 *urological cases*. J Urol, 2006. **175**(5): p. 1861-4.
- 908 55. Zacchè, M.M. and I. Giarenis, *Therapies in early development for the*  
909 *treatment of urinary tract inflammation*. Expert Opinion on Investigational  
910 Drugs, 2016. **25**(5): p. 531-540.
- 911 56. Geers, B., et al., *Crucial factors and emerging concepts in ultrasound-*  
912 *triggered drug delivery*. J Control Release, 2012. **164**(3): p. 248-55.
- 913 57. Khasriya, R., et al., *The spectrum of bacterial colonisation associated with*  
914 *urothelial cells from patients with chronic lower urinary tract symptoms*. J Clin  
915 Microbiol, 2013.
- 916 58. Guiton, P.S., et al., *Enterococcus faecalis overcomes foreign body-mediated*  
917 *inflammation to establish urinary tract infections*. Infect Immun, 2013. **81**(1):  
918 p. 329-39.
- 919 59. Poulsen, L.L., et al., *Enterococcus and Streptococcus spp. associated with*  
920 *chronic and self-medicated urinary tract infections in Vietnam*. BMC Infect  
921 Dis, 2012. **12**(1): p. 320.
- 922 60. Blomley, M.J.K., et al., *Microbubble contrast agents: a new era in ultrasound*.  
923 BMJ : British Medical Journal, 2001. **322**(7296): p. 1222-1225.
- 924 61. Caschera, L., et al., *Contrast agents in diagnostic imaging: Present and future*.  
925 Pharmacological Research, 2016. **110**: p. 65-75.
- 926 62. Roovers, S., et al., *The Role of Ultrasound-Driven Microbubble Dynamics in*  
927 *Drug Delivery: From Microbubble Fundamentals to Clinical Translation*.  
928 Langmuir, 2019.
- 929 63. Luan, Y., et al. *Liposome shedding from a vibrating microbubble on*  
930 *nanoseconds timescale*. in *2013 IEEE International Ultrasonics Symposium*  
931 *(IUS)*. 2013.
- 932 64. Madni, A., et al., *Liposomal drug delivery: a versatile platform for challenging*  
933 *clinical applications*. J Pharm Pharm Sci, 2014. **17**(3): p. 401-26.
- 934 65. Tranquart, F., T. Bettinger, and J.M. Hyvelin, *Ultrasound and microbubbles for*  
935 *treatment purposes: mechanisms and results*. Clinical and Translational  
936 Imaging, 2014. **2**(1): p. 89-97.
- 937 66. Vhora, I., et al., *Receptor-targeted drug delivery: current perspective and*  
938 *challenges*. Ther Deliv, 2014. **5**(9): p. 1007-24.
- 939 67. Raymond, I., et al., *The clinical effectiveness of intravesical sodium*  
940 *hyaluronate (cystistat(R)) in patients with interstitial cystitis/painful bladder*  
941 *syndrome and recurrent urinary tract infections*. Curr Urol, 2012. **6**(2): p. 93-8.
- 942

Figure 1

[Click here to download high resolution image](#)

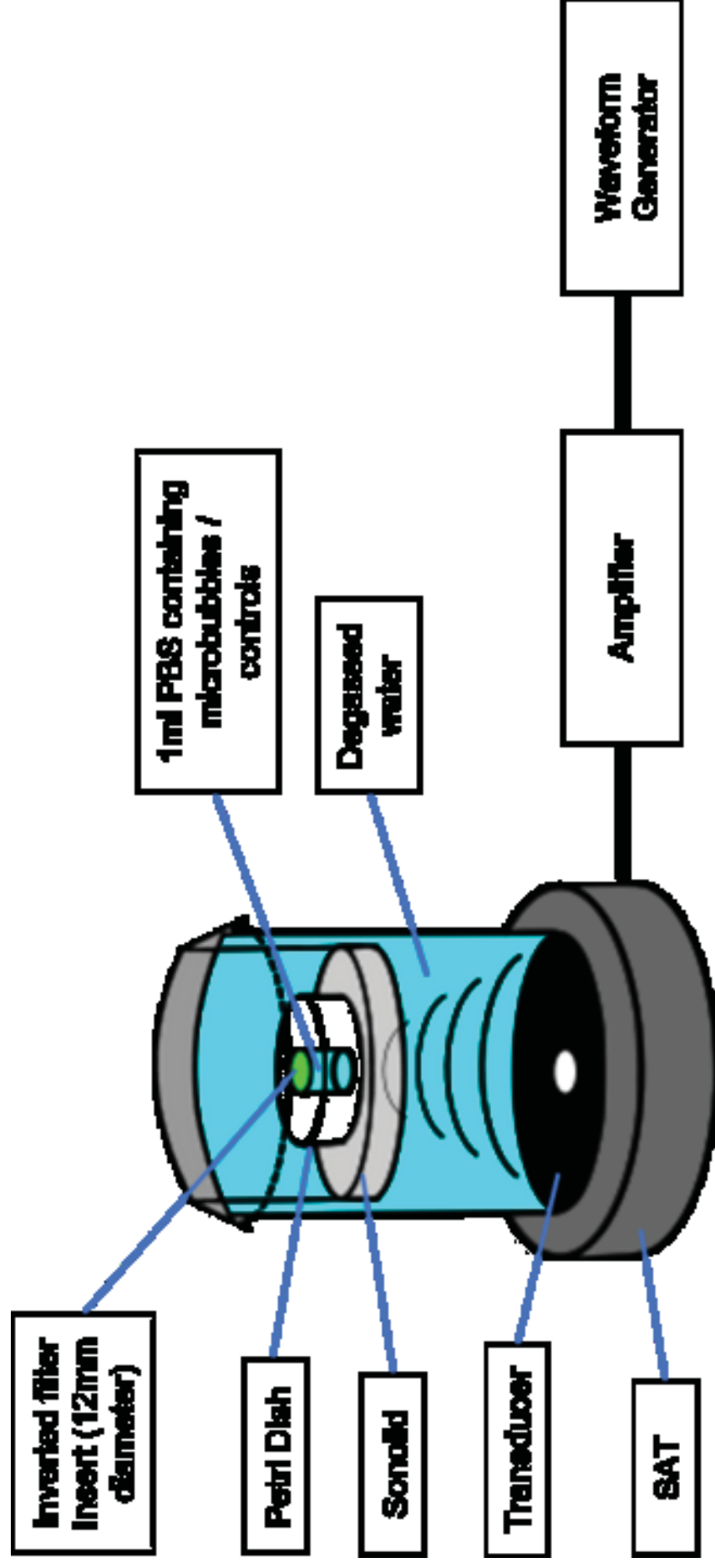


Figure 2  
[Click here to download high resolution image](#)

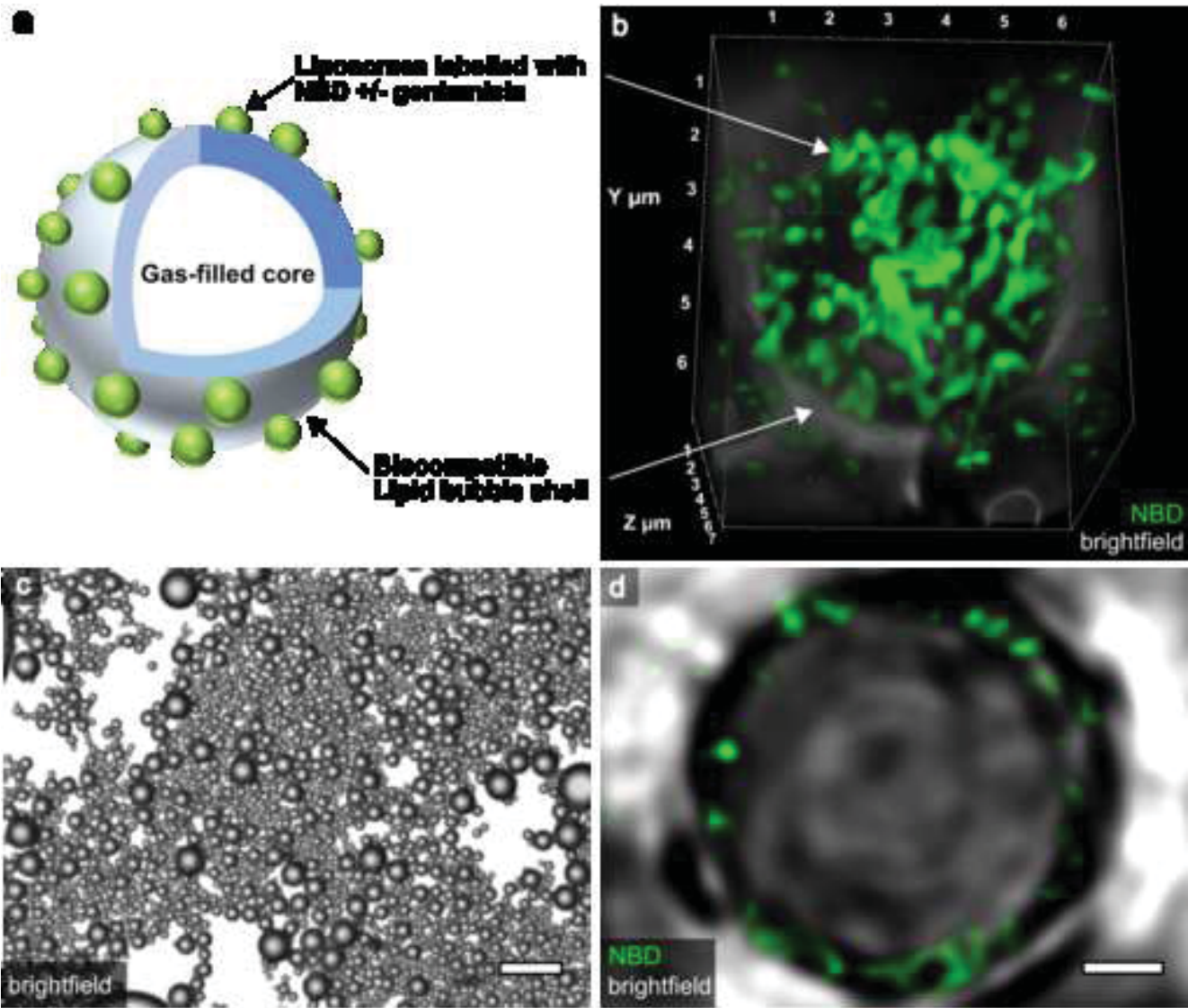


Figure 3  
[Click here to download high resolution image](#)

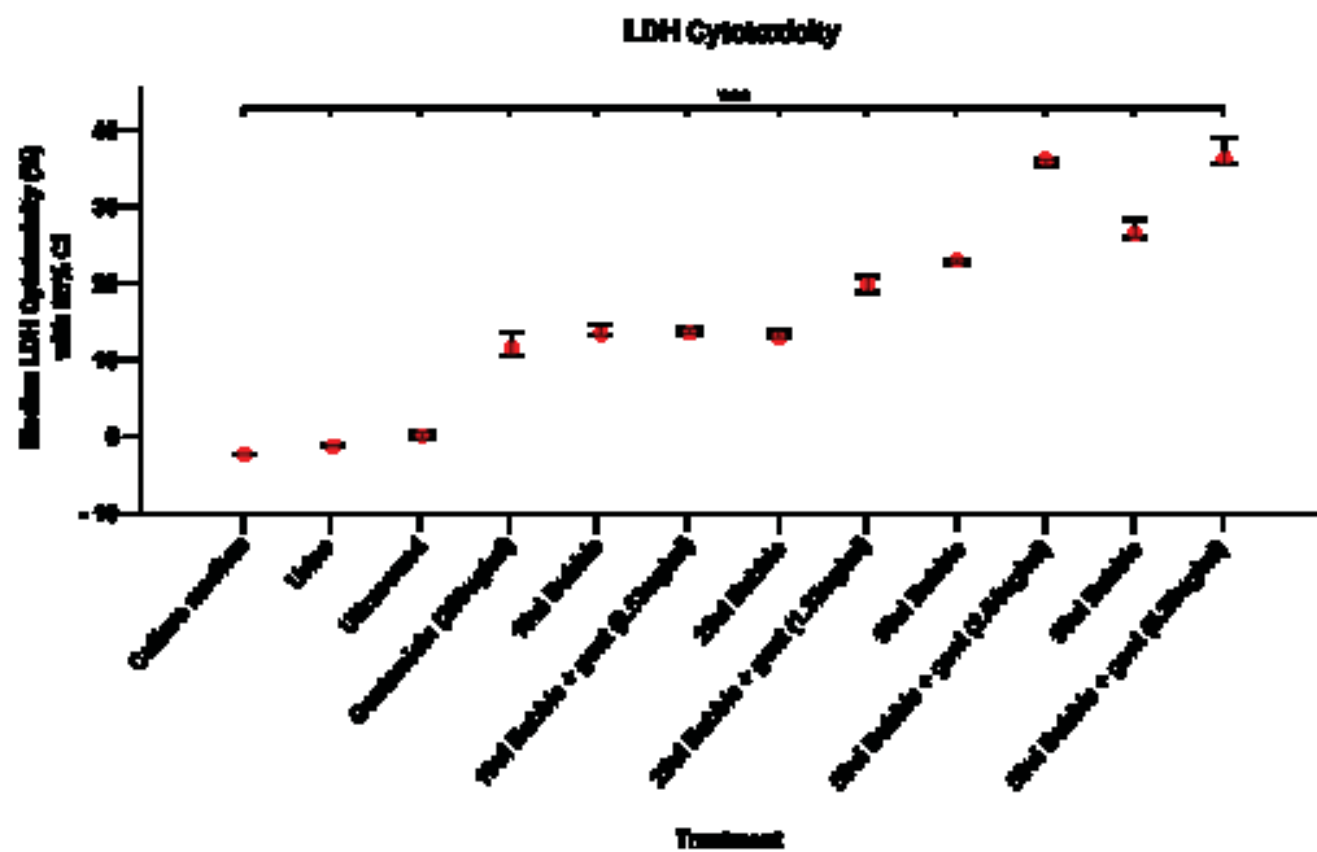


Figure 4  
[Click here to download high resolution image](#)

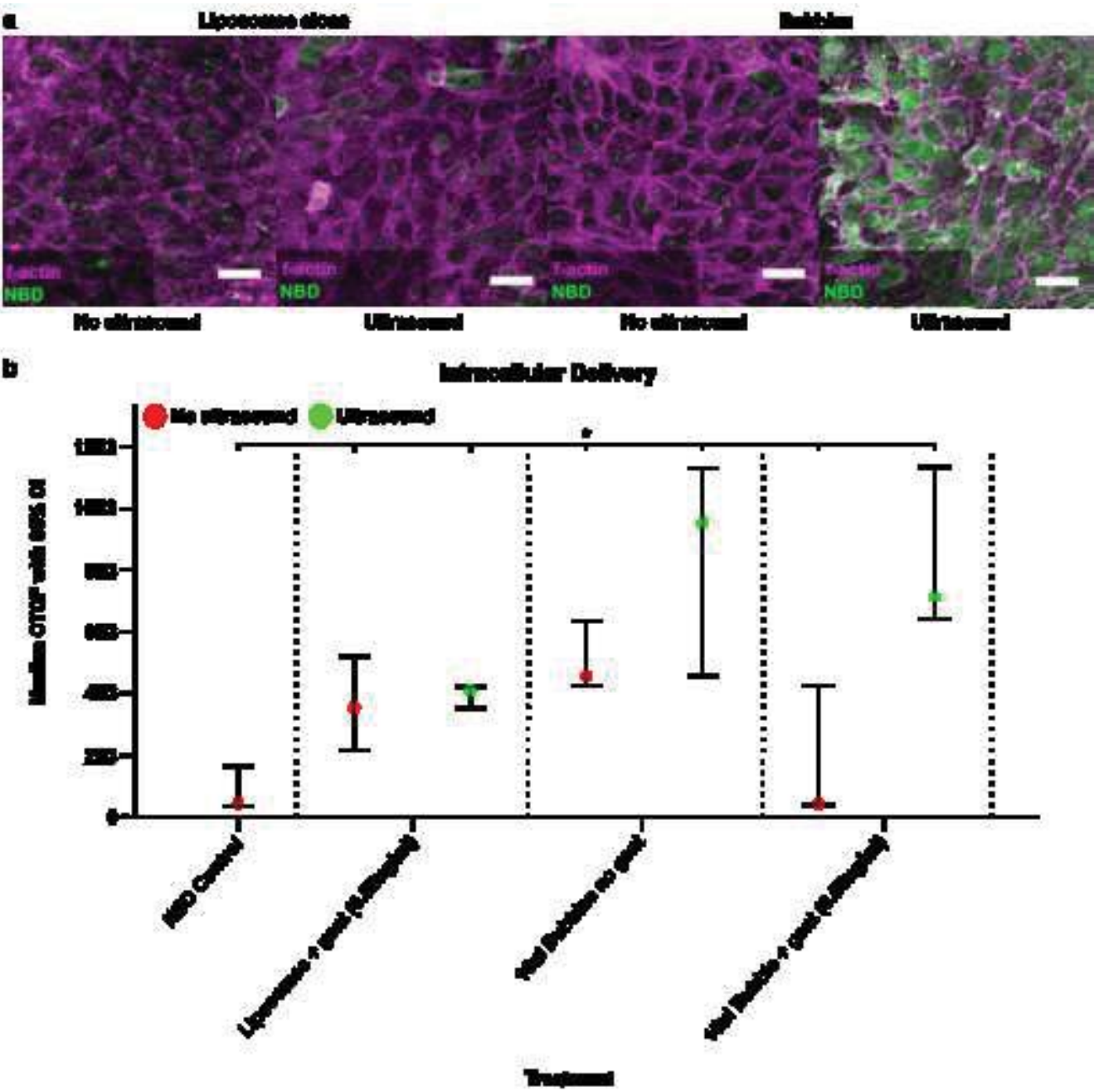


Figure 5  
[Click here to download high resolution image](#)

